Elucidating the Tertiary Structure of Protein Ions in Vacuo with Site Specific Photoinitiated Radical Reactions

ARTICLE *in* JOURNAL OF THE AMERICAN CHEMICAL SOCIETY · JUNE 2010

Impact Factor: 12.11 · DOI: 10.1021/ja910665d · Source: PubMed

2 AUTHORS:

Tony Ly
University of Dundee
25 PUBLICATIONS **665** CITATIONS
SEE PROFILE

Ryan R Julian
University of California, Riverside
96 PUBLICATIONS **2,023** CITATIONS
SEE PROFILE

Published in final edited form as:
J Am Chem Soc. 2010 June 30; 132(25): 8602–8609. doi:10.1021/ja910665d.

Elucidating the Tertiary Structure of Protein Ions *In Vacuo* with Site Specific Photo-initiated Radical Reactions

Tony Ly and **Ryan R. Julian***
Department of Chemistry, University of California, Riverside, CA 92521

Abstract

A new method for identifying residue specific through space contacts as a function of protein secondary and tertiary structure in the gas phase is presented. Photodissociation of a non-native carbon-iodine bond incorporated into Tyr59 of ubiquitin yields a radical site specifically at that residue. The subsequent radical migration is shown to be highly dependent on the structure of the protein. Radical-directed dissociation (RDD) of low charge states, which adopt compact structures, generates backbone fragmentation that is prominently distributed throughout the protein sequence, including residues that are distant in sequence from Tyr59. Higher charge states of ubiquitin, which adopt elongated, unfolded structures, yield RDD that is primarily nearby in sequence to Tyr59. Regardless of which structure is probed, information at the residue-level is obtained by examining specific radical-donor and radical-acceptor pairs. The relative importance of a particular interaction pair for a specific conformation can be revealed by tracking the charge state dependence of the dissociation. Structurally important contact pairs exhibit strong and concerted changes in relative intensities as a function of charge state and can also be used to reveal structural features which persist among different protein structures. Moreover, incorporation of distance constraint information into molecular mechanics conformational searches can be used to drive the search towards relevant conformational space. Implementation of this approach has revealed highly stable, previously undiscovered structures for the +4 and +6 charge states of ubiquitin, which bear little resemblance to the crystal structure.

Keywords

photodissociation; open-shell; electrospray ionization; migration; hydrogen atom transfer; gas phase; electrospray mass spectrometry; ion mobility

Introduction

Elucidation of protein structure is a challenging task in any setting and the gas phase, which is the ultimate low dielectric environment, is no exception. Upon desolvation of a protein, Coulombic interactions transition from playing a rather minor part to being a dominant factor controlling structure. As a result, the overall structure of a protein in the gas phase is highly dependent on charge state, with repulsive interactions consistently leading to greater unfolding for higher charge states. This effect has been demonstrated for numerous proteins in experiments utilizing ion mobility, which can easily measure the collision cross section or overall size of a protein.1⁻6 Nevertheless, more detailed information about protein structure, for example at the residue level, is very difficult to obtain. Ion molecule reactions, such as

*Correspondence should be addressed to: ryan.julian@ucr.edu.

Supporting Information Available. The supporting information contains the full citation for reference 16, Figures S1 – S3, and PDB coordinates for all calculated structures. This information is free of charge via the Internet at http://pubs.acs.org/.

gas phase H/D exchange, can yield information about exchangeability in distinct regions of a protein,[7–9] but the translation of such information into structure is typically very difficult. Various dissociation methods have also been explored as means for obtaining information about protein structure, although most have not succeeded.[10,11] Some success is afforded with electron capture dissociation (ECD), which has the potential to reveal hydrogen-bonding networks.[12–14] In these experiments, it is assumed that facile dissociation of the N-C_α bond occurs without rupturing noncovalent interactions;[15] therefore, regions where ECD fragments are observed as separated products likely do not have significant tertiary contacts to the remaining protein. Unfortunately, further examination of portions of the protein with significant tertiary contact is not possible.

Molecular modeling has also been used to evaluate gas phase protein structure, frequently in conjunction with experiment.[16–18] Due to the constraints imposed by the size of proteins and even large peptides, the level of theory for modeling is typically restricted to molecular mechanics. Modeling has been largely successful in evaluating the structures of peptides, where conformational space is somewhat restricted, when used in conjunction with ion mobility.[19,20] In proteins, however, the larger molecular size leads to an exceedingly vast number of potential structures, many of which have the same nominal cross sections and calculated energies. Given that collisional cross section is the only parameter experimentally measured, distinguishing which (or how many) of these conformers are correct is frequently not possible. Despite these limitations, ion mobility presently offers the best data for comparison with theory since incorporation of H/D exchange or ECD data into molecular mechanics simulations is not straightforward. Therefore, there remains a significant need for experimental methods that can reveal residue level information that can be unambiguously leveraged to obtain protein structure directly, or in combination with simulations.

Of all gas phase proteins, ubiquitin is one of the most often examined. Ion mobility measurements of protonated ubiquitin have shown that charge states greater than +8 have collisional cross sections that are consistent with elongated conformers whereas the +4 charge state has a collisional cross section that is compact and consistent with the crystal structure.[1] Intermediate charge states are mixtures of compact, partially folded, and elongated structures. These results suggest that for specific charge states, i.e. the +4 through the +6 charge states of ubiquitin, the condensed phase structure may be retained in the gas phase. H/D exchange results are consistent with the ion mobility distributions, indicating that low charge states are heterogeneous in structure whereas higher charge states are nearly homogeneous.[7] ECD of the +5 charge state yields no separated backbone fragments, suggesting that the structure is fully folded with significant tertiary contacts throughout.[12] ECD of the +6 charge state yields fragmentation between residues 1 through 14, and 74 through 76, suggesting that tertiary contact in these regions has been reduced. Although considerable information about the structure of ubiquitin has been acquired from all of these experiments, the actual gas phase structures for the various charge states remain unknown.

In the present manuscript, we report a new method for examining protein structure in the gas phase. This method relies on site-specific incorporation of a photolabile radical precursor at a tyrosine residue, followed by radical initiation, migration, and dissociation.[21] It is found that radical migration is highly sensitive to protein structure, and consequently, spatial proximity to the initial radical site dictates where radical directed dissociation (RDD) will occur. Experiments with ubiquitin reveal that radical migration to sites that are distant in sequence from Tyr59 (> 5 residues away) decreases significantly upon disruption of the tertiary structure. Moreover, radical transfers from Tyr59 to specific residues are highly structurally dependent. The charge-induced unfolding of ubiquitin proceeds by disruption of contacts between Tyr59 and the N-terminal portion of the protein and a significant rearrangement of the C2 terminal half. Radical transfer between Tyr59 and residues that are

distant in sequence indicate the presence of specific, through-space contacts. These experimentally derived contacts provide multiple constraints for both generating and validating structures with molecular mechanics. The structures identified by this methodology are stable towards 10 ns unconstrained molecular dynamics simulations, low in energy, and consistent with both the RDD data and cross sections obtained by ion mobility.

Experimental Methods

Materials

Bovine ubiquitin was purchased from Sigma Aldrich (St. Louis, MO). HPLC-grade acetonitrile, sodium iodide, chloramine-T hydrate, sodium metabisulfite and glacial acetic acid were purchased from Thermo Fisher Scientific (Waltham, MA). Water was purified to 18.2 MΩ resistivity using a Millipore Direct-Q (Millipore, Billerica, MA). Dialysis membranes and clips (MWCO = 3500) were purchased from Spectra Por (Rancho Dominguez, CA).

Chloramine-T Iodination of Proteins

Milligram quantities of protein are iodinated using sodium iodide as the iodine source, chloramine-T as the oxidant and sodium metabisulfite as the quenching reagent.21 Iodinated proteins are dialyzed against water and stored frozen in 50 nmol aliquots.

Electrospray Mass Spectrometry and Photodissociation

Solutions containing 10 μM of protein in 50/50 H_2O/acetonitrile + 0.5% acid are infused into the standard electrospray source of a Thermo LTQ linear quadrupole ion trap mass spectrometer. The back plate of the instrument is modified with a quartz window to transmit fourth-harmonic (266 nm) pulses from a flashlamp-pumped Nd:YAG laser (MiniLite, Continuum, Santa Clara, CA). Laser pulses are synchronized to a typical MS^2 activation step by enabling a diagnostic trigger in the LTQ Tune software, which delivers a 3.3V differential signal, which is converted to be a TTL pulse by a digital delay generator and sent to the laser at the beginning of each MS^2 activation period. Ions are isolated using an isolation width of 3 m/z units for photodissociation (PD). PD products (i.e. loss of iodine atom) are re-isolated using an isolation width of 10 m/z units and subjected to collision induced dissociation (CID). At a minimum, manual charge state assignment is attempted for all peaks >5% relative abundance using the zoom and ultrazoom scan modes of the LTQ, which can typically resolve the isotopic envelope of up to a + 8 ion. Charge states for many peaks below the 5% threshold were resolvable and assigned. Peaks in experimental spectra are assigned to backbone fragments with the aid of Fragmentor software (v. 1.0.0.3), which is available online at http://faculty.ucr.edu/ryanj/fragmentor.html. We adopted the standard nomenclature for peptide fragments and added the superscripts "*" and "°" to indicate NH_3 loss and H_2O loss, respectively (e.g., $b^*_{58} \equiv b_{58}$ - NH3). Assignments do not distinguish between closed shell vs. radical (e.g., −H·) fragments.

Molecular Modeling

The Maestro and MacroModel computing suite (Schrodinger Inc., San Diego, CA) was used to build models of protonated ubiquitin and perform all molecular modeling simulations. The OPLS atomic force fields is used for all calculations.22,23 The initial "seed" structure is derived from the atomic coordinates determined by x-ray crystallography (1UBI).24 All acidic residues are simulated as the charge neutral species. It is likely that the choice of protonation sites significantly affects the molecular modeling results. Therefore, we have referred to previous investigations on the protonation locations in ubiquitin.12,25 For the +4

charge state of ubiquitin, two of the charges reside on Arg42 and Arg54. The third charge is sequestered by one of the C-terminal arginines (Arg72 and Arg74). The last charge is flexible, and can be located on any lysine residue. Taking into consideration these probabilities, we have chosen Arg42, Arg54, Arg74 and Lys6. For the +6 charge state, we have chosen Lys6, Lys11, Lys33, Arg42, Arg54, and Arg74 as the charged sites.

Tertiary contact information obtained from RDD is implemented as 6 ± 1.5 Å distance constraints with force constants of 100 $kJ \cdot mol^{-1} \cdot Å^2$. The structure is subjected to 120 rounds of simulated annealing cycles that begin with a heating step to 2500 K (10 ps stochastic dynamics simulation), followed by several cooling steps (10 ps each) to a final bath temperature of 50 K. Additional simulated annealing experiments are performed until the last 120 rounds resulted in conformations with similar calculated energies. This process was repeated at incrementally lower initial temperatures (2000 K, 1500 K, 750 K, 300 K) to obtain lower energy structures.

Calculated Cross Sections

Cross sections are calculated using the exact hard spheres scattering approximation as implemented in the MOBCAL program, which was developed and currently maintained by the Jarrold laboratory at Indiana University.[26,27]

Results and Discussion

A photolabile carbon-iodine bond is incorporated into Tyr59 of ubiquitin using well-established iodination chemistry.[21] Irradiation of iodoubiquitin with a single pulse of 266 nm photons dissociates the carbon-iodine bond, as shown in Figure 1a, to yield a radical localized to a single carbon center on the side chain of tyrosine. The photodissociation yield for the +4 and +5 charge states of ubiquitin are unusually low (~12–17%) compared to higher charge states of ubiquitin, which are typically around ~30%. Photodissociation yields for the +4 through +10 charge states are shown in Figure S1 in the Supporting Information. The CID spectrum for the radical photoproduct $[(\text{Ubiquitin})\cdot + 5H]^{5+}$ is shown in Figure 1b. The key features of this spectrum are the a, c, and z fragment ions, which are absent in the CID spectrum of the even-electron protein.[28] As observed previously for the +6 charge state,[21] the most intense backbone fragmentation (e.g. c_{54}, a_{59}, a_{54}, c_{56}) is due to radical-directed dissociation (RDD) and occurs nearby in sequence to the initial radical site, Tyr59.

The relationship between amino acid sequence and backbone fragmentation is better illustrated by plotting the RDD backbone fragmentation intensities by residue number. Figure 2 shows the RDD fragmentation plots for charge states +4 through +10. Arginine and tyrosine side chain loss intensities are also included in Figure 2 at the residues from which these side chain losses were determined to originate. Although other side chain losses were observed, they are not incorporated into Figure 2 because residue specific information was not obtainable. RDD of the +4 charge state (Figure 2, top) results in fragmentation that is well-distributed across the ubiquitin sequence. The most prominent fragmentations are cleavage of the backbone bonds connecting Arg42 and Leu43, Asp21 and Thr22, and Val17 and Glu18. Interestingly, backbone fragmentation at these sites, and at other residues distant in sequence from Tyr59, decreases significantly with increasing charge state. In the +6 and +7 charge states prominent arginine side chain loss is observed from one of the C-terminal arginines (Arg72 or Arg74, vide infra) and backbone fragmentation at Tyr59 becomes abundant. It is clear that RDD fragmentation becomes increasingly localized to residues close in sequence to Tyr59 in the higher charge states. In addition, tyrosine side chain loss appears in the +8 charge state and becomes the nearly exclusive fragmentation product by the +10 charge state. These observations are all consistent with the idea that structure strongly influences RDD as will be detailed below.

Close inspection of Figure 2 reveals that the RDD fragmentation for the +4 charge state is significantly different from the +5. In contrast, the most abundant fragments in the CID spectra of the even-electron +4 and +5 charge states are identical, suggesting that RDD is sensitive even to modest variations in protein structure which do not influence CID.11 Changes in RDD fragmentation are most easily explained by differences in radical migration. In previous work, we have demonstrated that radical migration occurs easily if the reaction is exothermic and if the radical donor and acceptor can attain the proper orientation relative to one another.29 In proteins, both of these factors are functions of three dimensional structure. It is observed generally in Figure 2 that radical migration to residues distant in sequence from Tyr59 is facilitated in compact structures adopted by low charge states, and attenuated by the extended structures found for higher charge states. A quantitative treatment for these observations is provided in Figure 3, where the sum of all backbone fragmentation located more than five residues away from Tyr59 is shown as a function of charge state (blue squares). The sums are normalized to the +4 charge state. Distal fragmentation drops steeply from +4 to +7 and then decreases at a lower rate from +7 to +10. These two trends are consistent with the average collisional cross sections measured by ion mobility, which are shown as red triangles.1 The degree of radical migration that is distant in sequence from Tyr59 in ubiquitin is therefore clearly correlated with overall protein size.

Radical migration through-space and through-sequence

Radical transfer proceeds either through-space or through-sequence until the radical reaches a destination where backbone fragmentation or side chain loss is favorable. In proteins, these locations are abundant and likely limit the maximum number of consecutive radical transfers. The theoretical limit can be estimated by calculating the probability that a random hydrogen atom abstraction reaction will occur at a site that will induce fragmentation. Sites that induce fragmentation have been identified previously by examining the mechanisms of backbone fragmentation and side chain losses observed in peptides.29,30 In ubiquitin, the number of carbon-bound hydrogen atoms capable of being abstracted by the initial radical based on reaction enthalpy is 470. Upon abstraction, 285 of the subsequent carbon-centered radicals are expected from previous experiments to dissociate into observable products such as backbone fragmentation and side chain loss.30 Thus, in the absence of structural effects, there is a ~60% probability that the first transfer places the radical in a site susceptible to fragmentation and the probability increases to ~94% by three radical transfers. This simple model does not take into account several important points. First, the number of possible exothermic hydrogen atom abstractions decreases significantly after the first transfer.30 Moreover, only the first radical transfer from the tyrosyl radical to an α or β carbon is predicted by theory to be potentially barrierless.29 Consistent with this prediction are the differences in reactivity observed between radical peptides and radical tyrosine with molecular oxygen, which indicate that radical migration is fast (< ms) and occurs without additional collisional activation.31 Barriers to subsequent transfers (such as between the α and β carbons) are typically moderate in the absence of structural constraints. In reality, structural effects cannot be ignored and will likely limit migration to donor/acceptor pairs which are in close contact. Therefore, the statistically predicted maximum of three radical transfers is probably an overestimate. Migration to residues that are distant in sequence from Tyr59, for example to Thr66, Thr22, and Thr14 in the +4 and +5 charge states, most likely occurs via through-space migration because an improbably high number of radical transfers would be required otherwise.

Tertiary Contacts Direct Radical Fragmentation of Distal Side chains

Examination of side chain losses reveals additional structural information. Side chain losses in the low charge states (+4 and +5) appear facile and result in peaks corresponding to loss

of multiple side chains, shown in the trailing edge of the precursor m/z in Figure 1a. In contrast, an intense fragment corresponding to loss of 87 Da is observed for the +6 charge state, as shown in Figure 4a. Loss of 87 Da has been observed previously in peptides, and originates from cleavage of the arginine sidechain.29,30 Further tandem MS experiments reveal the location of the arginine from which side chain loss occurs. CID of [Ubiquitin + 5H – 86]$^{5+}$, shown in Figure 4b, yields [y_{24} + 2H – 86]$^{2+}$, which limits the side chain loss to three arginines: Arg54, Arg72 and Arg74. Further MS on the y_{24} fragment (inset) yields a pseudo b_6 fragment ion containing the residues Gly53 through Asp57, which eliminates Arg54 as a candidate. Thus, Arg72 and Arg74 are the only remaining candidates. These results indicate that there is significant interaction between Tyr59 and the C-terminus in the +6 charge state.

A tertiary contact between Tyr59 and Arg74 is consistent with ECD studies of the +6 charge state of ubiquitin.12 Interestingly, separated products due to cleavage between residues 14 and 74 are absent, indicating the existence of tertiary structure in this region. This tertiary interaction disappears with additional charges, as indicated by increased ECD fragmentation in the C-terminal region and a substantial decrease in arginine side chain loss in the RDD. Arginine side chain loss occurs in competition with many other processes. As shown in Figure 4d, the highest fractional yield of arginine side chain loss for any charge state is 20% (+6 charge state). Tyrosine side chain loss, on the other hand, can be much more abundant as will be explained presently.

Fragmentation in high charge states is marked by abundant loss of tyrosine side chain. For example, the most abundant RDD peak for [(Ubiquitin)· + 10H]$^{10+\cdot}$ is tyrosine side chain loss (−106), as shown in Figure 4c. We have previously demonstrated that the 106 loss from tyrosine is due to a strained 1,3 hydrogen atom transfer from the hydroxyl to the *ortho* radical on tyrosine.29 This strained migration is likely disfavored when alternate exit channels exist. Abundant loss of 106 therefore suggests that tyrosine is isolated in the +10 charge state, and that secondary and tertiary contacts with the remaining protein are minimal. Consistent with this interpretation is the increase of tyrosine side chain loss with increasing charge, as shown in Figure 4d. Here, the fractional abundances of tyrosine and protonated arginine side chain loss are shown as a function of charge state. The y-axis represents the fraction of the specific side chain loss relative to the sum of all side chain losses. Although loss of tyrosine side chain is the most abundant fragment in the +10 charge state, retention of backbone fragmentation at Thr55 and Asp58, i.e. the presence of the a_{54} and a_{58} fragment ions in Figure 4c, indicate that there remains a low probability for radical transfer from the tyrosine side chain to nearby residues.

Resolution of Conformational Classes

Closer examination of intense RDD fragments as a function of charge state reveals additional trends. Figure 5 plots the intensities of key backbone and side chain fragments versus charge state, as extracted from the data in Figure 2. It can be observed that the fragmentation intensities at Ile13/Thr14 and Asp21/Thr22 are highest in the +4 charge state and decrease along similar trajectories from +4 to +6, as shown in Figure 5a. Backbone fragmentation at these two locations disappears completely above the +7 charge state. These results indicate that low charge states are populated by conformations that favor radical migration to the N-terminal half of ubiquitin. Moreover, the unfolding event that mitigates migration to Thr14 also prevents migration to Thr22. Fragmentation at Ser65/Thr66 also decreases with increasing charge state, but persists through the +7 charge state. Together these results suggest that protonation disrupts tertiary contacts to the N-terminal half of ubiquitin at the same time as the C-terminal half is undergoing structural reorganization. Indeed, the appearance of arginine side chain loss and backbone fragmentation at Asp58, Tyr59, and Asn60 in the +6 and +7 charge states suggests that the C-terminal half has

restructured to favor radical migration to these sites. Backbone fragmentation intensities at Asp58, Tyr59 and Asn60 together follow the same trend, with maxima at the +7 charge state.

In contrast, the intensity of arginine side chain loss, shown in Figure 5c does not correlate with these backbone fragments or with any other fragmentation pathway. The lack of correlation suggests that a significant population of the +6 ions are structurally unique and do not appear in other charge states. In contrast, fragmentation at Arg54/Thr55 exhibits a unique charge state dependence which spans across several charge states, as shown in Figure 5c. Facile radical migration to Thr55 precludes secondary structures that contain an extended backbone or prevent direct contact between Thr55 and Tyr59, such as the β sheet structural motif. These structures would mitigate through-space and through-sequence transfers to Thr55. It is also unlikely that the gas phase secondary structure mimics the 3_{10} helix found in the condensed phase in this region of the protein, which places the side chain of Tyr59 on the opposite face of the helix as Thr55.24 Instead, facile radical migration between residues separated by four amino acids in sequence is consistent with an α helix or a random coil. Our results therefore suggest that the secondary structure in this region is distorted from the solution structure and persistent through a number of different tertiary motifs.

Application to Conformational Searching—Molecular mechanics simulations have been used extensively in conjunction with gas phase techniques to study the structure of proteins.16–18 Experimentally determined proximities between Tyr59 and other residues revealed by RDD can be implemented in molecular mechanics simulations as distance constraints. Theory predicts that abstraction of the C_α hydrogen atom from glycine by tyrosyl radical requires that the radical donating carbon atom be within 2.7 Å of the C_α of glycine.29 Therefore, what is likely measured in RDD experiments is the frequency of short-range contact, which is related to the equilibrium distance separating the two residues and the dynamic motion of the protein.

The +4 charge state adopts compact conformations exclusively, as determined by ion mobility. The cross sectional distribution, which has maxima at 1004 and 1059 $Å^2$, is similar to the theoretical cross section calculated for the x-ray crystal structure (1059 $Å^2$). Figure 6a shows the crystal structure of ubiquitin colored by RDD fragmentation intensity. The C_Z on Tyr59 is within 6 Å of the β carbons of Leu50, Glu51, Arg54, and Asp58. Limited RDD fragmentation is observed at these residues, and the most intense RDD fragments are at locations that are distant through-space from Tyr59. Numerous consecutive radical transfers would be required to explain the most intense RDD fragmentation, which as discussed above, are unlikely to occur. The incongruity between the gas phase data and the crystal structure suggests that the +4 charge state is populated by conformers that are structurally distinct from those found in the condensed phase. A molecular dynamics/simulated annealing (MDSA) approach was used to find structures that are consistent with the RDD results. Figure 6b shows the output of an MDSA calculation of the +4 charge state of ubiquitin (PDB-formatted coordinates are available in supporting information). The distances between Tyr59 and four residues where the most intense RDD fragments occur (Arg42, Thr22, Val17, and Thr66) were initially constrained to 6 Å ± 1.5 Å (see Experimental section). These constraints are represented in Figure 6b as green dotted lines. Molecular mechanics (MM) energies and key inter-residue distances for calculated structures are summarized in Table 1. The best-fit structure was stable towards a 10 ns stochastic dynamics simulation without distance constraints. Structures were sampled every 10 ps, yielding 1000 structures in total. The root-mean-square deviations (RMSDs) relative to the ‘best-fit’ structure are shown in Figure S2. The low average RMSD (1.3 Å) indicates that removal of the distance constraints does not destabilize the best-fit structure.

The secondary and tertiary structural elements that characterize condensed phase ubiquitin are absent in the best-fit structure and the backbone is significantly distorted relative to the crystal structure. Consistent with these qualitative observations is a calculated root mean square deviation (RMSD) of 13.5 Å between the structures shown in Figures 6a and b. Interestingly, the N- and C-termini interact in a pincer-like fashion in Figure 6b, which is consistent with structural data from ECD.12 Closer inspection of the best-fit structure indicates that solvation of the charged sites is a dominant factor in this *in vacuo* protein structure. Although the pronounced effect of charge-charge repulsive interactions on structure is well-documented, the combined MDSA and RDD results indicate that favorable electrostatic interactions influence the organization of protein structure at lower charge states significantly. As shown in Table 1, the calculated MM energy for the best-fit structure is lower than the crystal structure by 625 kJ/mol. The difference in energy is due to a stabilization of electrostatic interactions (−531 kJ/mol) in the best-fit structure and a modest stabilization of the van der Waals interactions (−100 kJ/mol). The decrease in electrostatic energy is due in part to the significant rearrangement of the backbone structure surrounding the charged residues in order to better solvate the positive charges. Indeed, the local structure surrounding charged residues are loop-regions, where backbone carbonyls and polar side chains are oriented toward the charges.

Despite significant differences in structure and calculated MM energies between Figures 6a and b, the two conformations would be difficult to distinguish using ion mobility. For example, the calculated cross sections for the best-fit and crystal structures are 1059 $Å^2$ and 1075 $Å^2$, respectively. The 1.5% relative difference is within the trial-to-trial error reported previously for ubiquitin cross sections.[1,4,6] Moreover, an MDSA approach without guidance from residue-resolution experimental constraints would have a significantly smaller chance of successfully finding the best-fit structure. Indeed, the MDSA experiment repeated without distance constraints resulted in a structurally distinct conformer (13 Å RMSD relative to Figure 6a) that has a calculated collisional cross section of 1067 $Å^2$. The color-coded calculated structure, shown in Figure 6c, indicates that structure is inconsistent with the most intense RDD fragmentation pathways. However, the structure is consistent with numerous less intense RDD fragmentations, including at residues Asp32, Ile36 and Glu64. The distances between Tyr59 and these residues are 5.4 Å, 4.4 Å, and 4.0 Å, respectively. Interestingly, the distances to these residues are much greater in the best-fit structure (12.3 Å, 13.3 Å, and 14.0 Å).

A quantitative model is useful to evaluate which structures are most consistent with the observed RDD fragmentation. The following scoring algorithm (equation 1) was developed to quantify the quality of the fit between the calculated structures and the RDD fragmentation data,

$$\frac{\sum_{i=1}^{76} x_i \cdot I_{RDD}}{\sum_{i=1}^{76} I_{RDD}} = X_{corr} \quad (1)$$

where x_i is 1 if the i^{th} residue is within 10 Å of Tyr59 in the calculated structure and 0 if not, I_{RDD} is the relative RDD fragmentation intensity at residue i, and X_{corr} is the correlation score. Thus, X_{corr} of 1.0 is obtained when all residues where RDD fragmentation occurs are within 10 Å of Tyr59, indicating perfect correlation between the calculated structure and the RDD data. The score for a 'random structure' of ubiquitin was also calculated. Here, Tyr59 was randomly assigned to be near 10 – 25 residues and correlated with the RDD data. The

average score of 1×10^6 trials is 0.225, with a standard deviation of 0.092. Therefore, only calculated structures with scores greater than ~ 0.32 are significantly better fits than a random structure. The scores for all calculated structures are listed in Table 1. The scores for the crystal structure and the unconstrained structures (both 0.30), indicate that these structures are poorly correlated with the RDD fragmentation. The score for the constrained structure is significantly higher than the crystal structure (0.47), but captures less than half of the RDD fragmentations. The low score is not surprising considering the wide sequence distribution of RDD fragmentation, which would be difficult to explain with a single structure. Instead, these results are consistent with heterogeneous tertiary interactions surrounding Tyr59, and imply that multiple structures exist as compact conformers in the gas phase.

According to ion mobility, the +6 charge state adopts a broad distribution of compact and partially unfolded conformations, with slight maxima at 1041 $Å^2$ and 1220 $Å^2$, respectively. 1 Figure 6d shows the crystal structure with the RDD data from the +6 charge state superimposed. The most striking difference between the RDD fragmentation and the crystal structure is the large separation between the C-terminus and Tyr59 (Tyr59 to Arg74 distance is 21.5 Å). Interestingly, this difference would easily be resolved if the C-terminal tail pivoted towards Tyr59, which would also require disruption of the cross β-sheet structure between the C-terminal tail and residues 42 through 45. This ‘rearranged’ structure was modeled computationally and subjected to a 20 ns molecular dynamics simulation. The MM energy for the final, minimized structure (shown in Figure S3) is −10982 kJ/mol, which is comparable to the energy calculated for alternative structures (vide infra). Tyr59 and Arg74 are in close proximity (3.8 Å inter-residue distance); however, Thr55, Thr66, and His68 are separated from Tyr59 by 11.7 Å, 13.7 Å and 12.5 Å, respectively. Importantly, the fragmentation at Thr66 and His68 is not easily explained by either the crystal structure, or simple rearrangement of the C-terminal tail.

Figure 6e shows the result of the MDSA calculation on the +6 charge state with distance constraints imposed between Tyr59 and Arg74, Thr55, Thr66 and His68. Arg74 was chosen as the protonation site for the MDSA calculation; however, Arg72 is an equally probable choice.9 To test whether this choice significantly affects the modeling results, we moved the charge from Arg74 to Arg72 in the output structure and subjected it to a 10 ns MD simulation. The RMSD between the final structure obtained by MD and the structure in Figure 6e is 2.4 Å, indicating that small shifts in protonation location (i.e. Arg74 → Arg72) do not significantly affect the stability of the calculated structure.

As observed for the +4 charge state, the +6 structure is significantly distorted relative to the crystal structure. The calculated cross section for the ‘best-fit’ structure is 1129 $Å^2$. The calculated cross section falls within the distribution measured by ion mobility.1 Figure 6f shows the output of an unconstrained MDSA search. Comparison of the N-terminal domains in Figures 6e and f reveal that both are relatively compact and consist of loop regions that facilitate solvation of positive charges by the backbone. However, the specific backbone carbonyls that participate in charge solvation are different and indicate that there is more than one stable permutation of backbone-charge interactions. Inter-conversion between the two structures may require substantial activation energy to shift charge solvation sites, but the relative energies of the conformations (at least at the MM level) suggest that both might exist. Indeed the more open conformation may represent the partially unfolded structure observed in ion mobility experiments; however, the RDD data suggests that this is not the dominant conformer observed in an ion trap. It is straightforward to envision combined ion mobility/radical migration experiments that would enable examination of such possibilities.

Evaluation of the 'fitting' scores for the calculated structures for the +6 charge state in Table 1 indicates that the constrained structure is most correlated with RDD fragmentation (score: 0.86). All other calculated structures score lower and have higher MM energies. Unlike the +4 charge state where multiple conformers are required to explain the RDD fragmentation results, the high correlation between the RDD fragmentation and the constrained structure suggests that tertiary interactions near Tyr59 are nearly homogeneous for the conformer(s) adopted in the +6 charge state.

Conclusions and Outlook

We have shown that radical migration is a sensitive probe of the gas phase structure of proteins. Different conformations of ubiquitin were sampled in the gas phase by examining different charge states. Low charge states are populated by numerous conformers that contain significant secondary and tertiary structure which facilitates through-space radical migration from Tyr59 to residues that are distant in sequence. In contrast, radical migration is significantly attenuated in higher charge states, which are known to have extended backbone structures. More specific information is obtained by examining where radical-directed fragmentation occurs, which reveals short-range contacts between Tyr59 and the site of dissociation. Residue-level structural information obtained by radical migration can be used as structural constraints which aid conformational search algorithms. These initial results suggest that radical migration is a promising novel method to examine the gas phase structure of proteins with residue resolution.

Distance-dependent transfer has been used with remarkable success to study protein structure in the condensed phase. Quantitative models of transfer of excitation energy and electrons have been developed and are used in conjunction with experimental methods to examine protein structural dynamics with high resolution. Similarly, the precision of the RDD technique would be significantly improved if a quantitative model of hydrogen atom transfer is determined, which connects fragmentation intensities and rates to the equilibrium distance between two residues. Such a model would permit elucidation of gaseous protein structure with an unprecedented level of detail.

Supplementary Material

Refer to Web version on PubMed Central for supplementary material.

Acknowledgments

RRJ acknowledges funding from the National Science Foundation (CHE-074748) and the National Institute of General Medical Sciences (R01GM084106) and TL acknowledges funding from the American Chemical Society Analytical Division Summer Fellowship sponsored by Eastman Chemicals and the UC Riverside Dean's Dissertation Award. We thank Evan Williams (UC Berkeley) and Chia-en Chang (UC Riverside) for insightful discussions.

References

1. Valentine SJ, Counterman AE, Clemmer DE. J. Am. Soc. Mass Spectrom. 1997; 8:954–961.
2. Shelimov KB, Clemmer DE, Hudgins RR, Jarrold MF. J. Am. Chem. Soc. 1997; 119:2240–2248.
3. Clemmer DE, Hudgins RR, Jarrold MF. J. Am. Chem. Soc. 1995; 117:10141–10142.
4. Hoaglund CS, Valentine SJ, Sporleder CR, Reilly JP, Clemmer DE. Anal. Chem. 1998; 70:2236–2242. [PubMed: 9624897]
5. Purves RW, Barnett DA, Ells B, Guevremont R. J. Am. Soc. Mass Spectrom. 2000; 11:738–745. [PubMed: 10937797]
6. Myung S, Badman ER, Lee YJ, Clemmer DE. J. Phys. Chem. A. 2002; 106:9976–9982.

7. Freitas MA, Hendrickson CL, Emmett MR, Marshall AG. Int. J. Mass Spectrom. 1999; 185/186/187:565–575.
8. Suckau D, Shi Y, Beu SC, Senko MW, Quinn JP, Wampler FM, McLafferty FW. Proc. Natl. Acad. Sci. U. S. A. 1993; 90:790–793. [PubMed: 8381533]
9. Gross DS, Schnier PD, Rodriguez-Cruz SE, Fagerquist CK, Williams ER. Proc. Natl. Acad. Sci. U. S. A. 1996; 93:3143–3148. [PubMed: 8610183]
10. Demmers JAA, Rijkers DTS, Haverkamp J, Killian JA, Heck AJR. J. Am. Chem. Soc. 2002; 124:11191–11198. [PubMed: 12224967]
11. Reid GE, Wu J, Chrisman PA, Wells JM, McLuckey SA. Anal. Chem. 2001; 73:3274–3281. [PubMed: 11476225]
12. Breuker K, Oh HB, Horn DM, Cerda BA, McLafferty FW. J. Am. Chem. Soc. 2002; 124:6407–6420. [PubMed: 12033872]
13. Horn DM, Breuker K, Frank AJ, McLafferty FW. J. Am. Chem. Soc. 2001; 123:9792–9799. [PubMed: 11583540]
14. Oh H, Breuker K, Sze SK, Ge Y, Carpenter BK, McLafferty FW. Proc. Natl. Acad. Sci. U. S. A. 2002; 99:15863–15868. [PubMed: 12444260]
15. McLafferty FW, Horn DM, Breuker K, Ge Y, Lewis MA, Cerda B, Zubarev RA, Carpenter BK. J. Am. Soc. Mass Spec. 2001; 12:245–249.
16. Bohrer BC, Merenbloom SI, Koeniger SL, Hilderbrand AE, Clemmer DE. Annu. Rev. Anal. Chem. 2008; 1:293–327.
17. Bernstein SL, Liu DF, Wyttenbach T, Bowers MT, Lee JC, Gray HB, Winkler JR. J. Am. Soc. Mass Spectrom. 2004; 15:1435–1443. [PubMed: 15465356]
18. Wu C, Murray MM, Bernstein SL, Condron MM, Bitan G, Shea JE, Bowers MT. J. Mol. Biol. 2009; 387:492–501. [PubMed: 19356595]
19. Wyttenbach T, von Helden G, Bowers MT. J. Am. Chem. Soc. 1996; 118:8355–8364.
20. Hudgins RR, Ratner MA, Jarrold MF. J. Am. Chem. Soc. 1998; 120:12974–12975.
21. Ly T, Julian RR. J. Am. Chem. Soc. 2008; 130:351–358. [PubMed: 18078340]
22. Jorgensen WL, Tirado-Rives J. J. Am. Chem. Soc. 1988; 110:1657–1666.
23. Jorgensen WL, Maxwell DS, Tirado-Rives J. J. Am. Chem. Soc. 1996; 118:11225–11236.
24. Vijay-kumar S, Bugg CE, Cook WJ. J. Mol. Biol. 1987; 194:531–544. [PubMed: 3041007]
25. Schnier PD, Gross DS, Williams ER. J. Am. Soc. Mass Spectrom. 1995; 6:1086–1097.
26. Mesleh MF, Hunter JM, Shvartsburg AA, Schatz GC, Jarrold MF. J. Phys. Chem. 1996; 100:16082–16086.
27. Shvartsburg AA, Jarrold MF. Chem. Phys. Lett. 1996; 261:86–91.
28. Reid GE, Wu J, Chrisman PA, Wells JM, McLuckey SA. Anal. Chem. 2001; 73:3274–3281. [PubMed: 11476225]
29. Ly T, Julian RR. J. Am. Soc. Mass Spectrom. 2009; 20:1148–1158. [PubMed: 19286394]
30. Sun Q, Nelson H, Ly T, Stoltz BM, Julian RR. J. Proteome Res. 2008; 8:958–966. [PubMed: 19113886]
31. Moore BN, Blanksby SJ, Julian RR. Chem. Comm. 2009:5015–5017. [PubMed: 19668834]

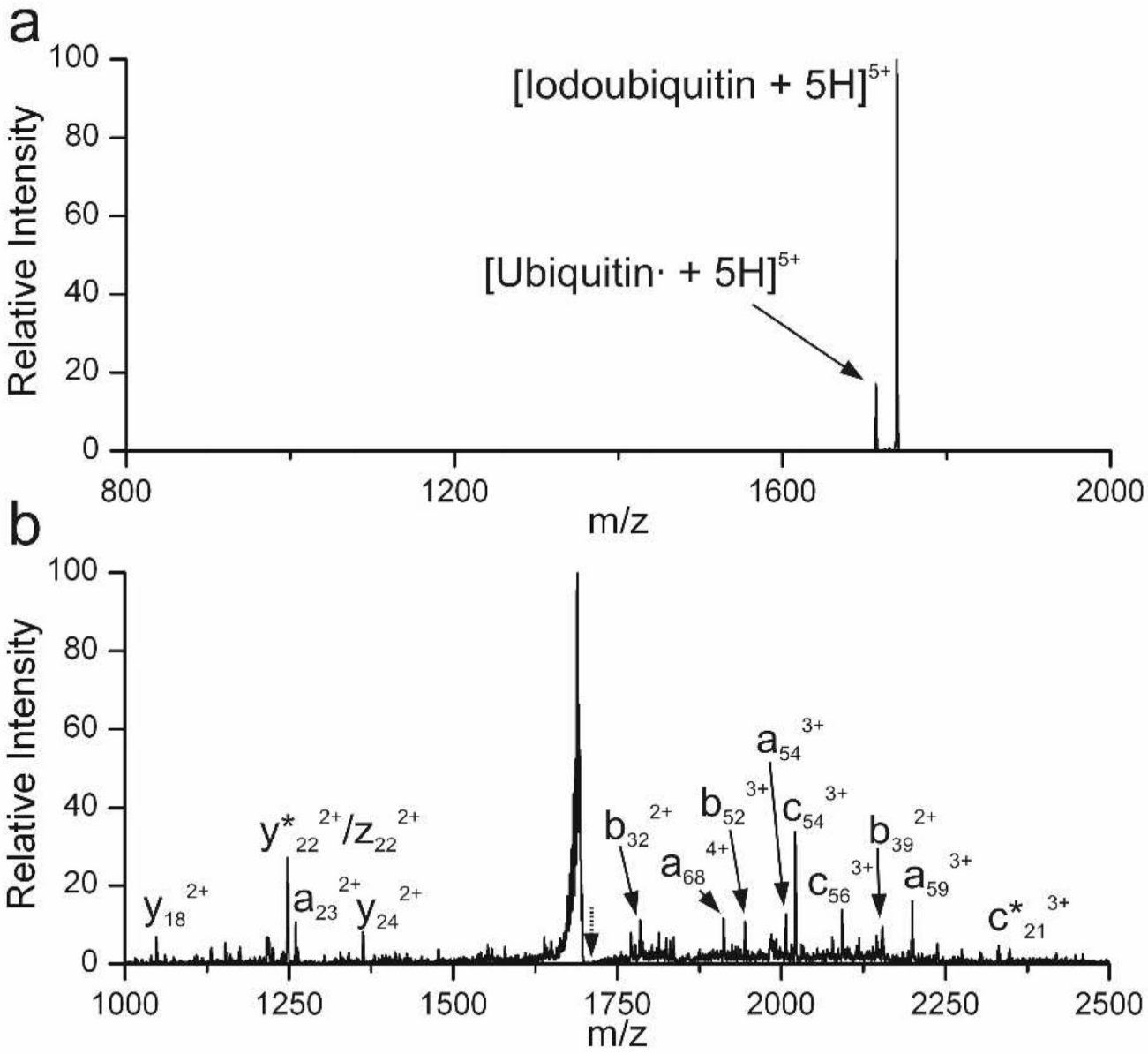

Figure 1.

a) Photodissociation of the +5 charge state of iodoubiquitin cleaves the iodine atom, yielding a protein radical ion. b) Collision induced dissociation of the radical product from (a), yields prominent radical-directed backbone fragment ions of the a, c, and z varieties. Dotted arrow indicates precursor m/z.

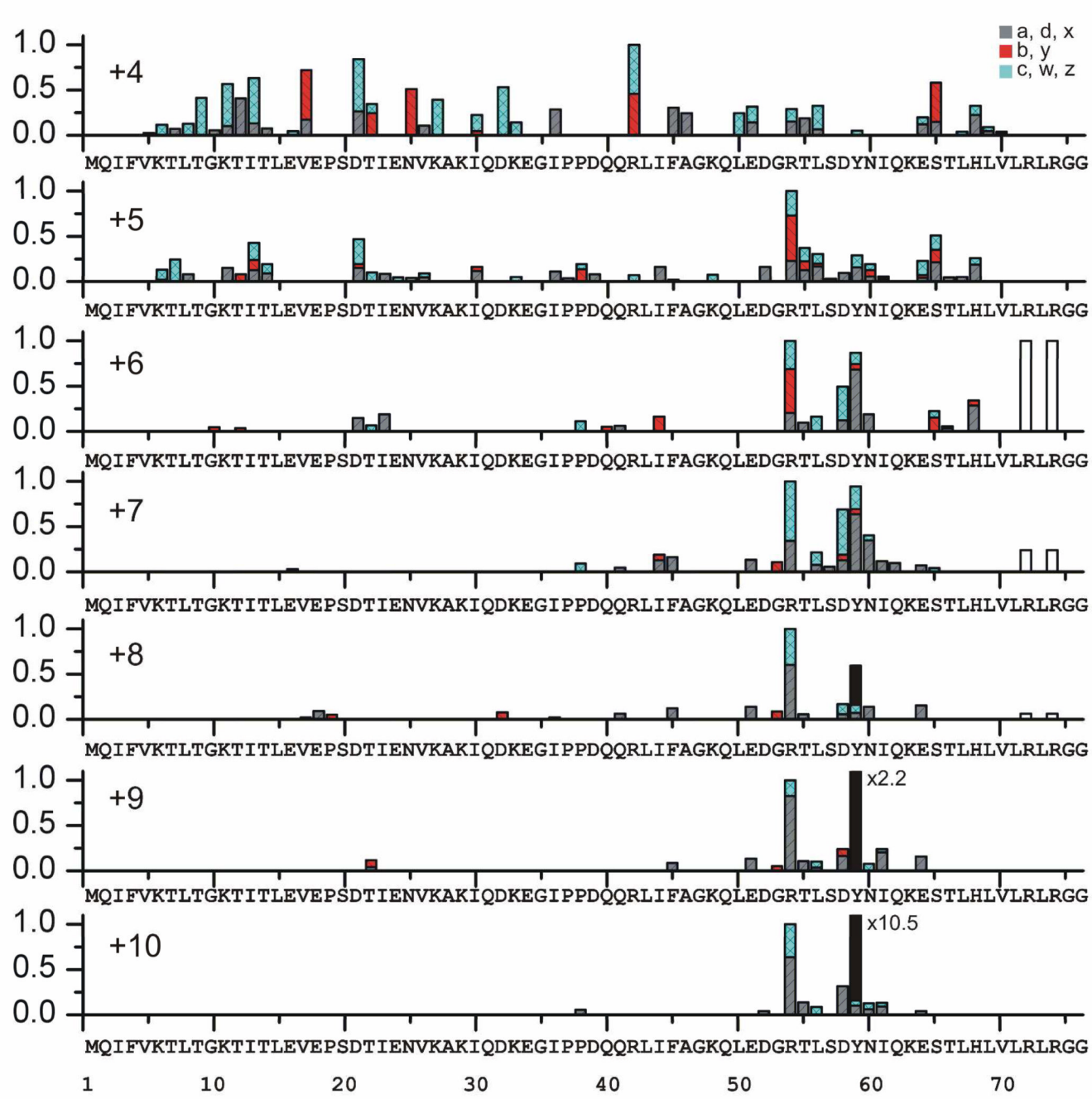

Figure 2.

Plots of radical-directed fragmentation as a function of sequence for charge states +4 through +10. Arginine and tyrosine side chain loss intensities are shown as white and black bars, respectively. For each charge state, the sum of RDD backbone fragmentation at each residue and side chain loss intensities are normalized to the highest sum.

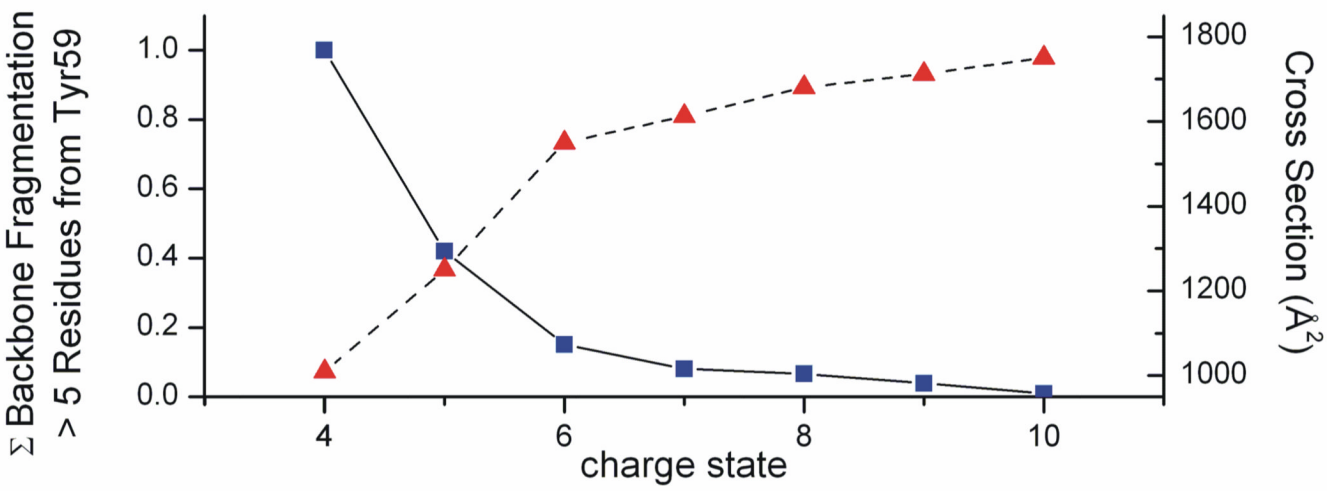

Figure 3.

Comparison of backbone fragmentation distant from Tyr59 (> 5 residues) summed for each charge state (squares) and the average collisional cross section from ion mobility data (triangles).1 Fragmentation at distal sites decreases significantly with increasing charge. The inverse relationship with the average collisional cross sections indicates that radical migration to residues that are distant in sequence from Tyr59 diminishes as the protein adopts more elongated structures.

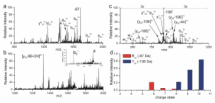

Figure 4.

a) CID of $[(\text{Ubiquitin})\cdot + 6\text{H}]^{6+}$ yields loss of protonated arginine side chain (−87) as the most intense fragment ion. Further MS/MS experiments locate the arginine residue from which the −87 loss originates. b) CID of −87 Da product yields an 86 Da-shifted y24 fragment ion, which narrows the loss to Arg54, Arg72, and Arg74. CID of the y_{24} fragment in (b) yields a prominent pseudo b_6 ion containing residues Gly53 through Asp57, which eliminates Arg54 as a candidate (inset). Thus, the side chain loss originates from either Arg72 or Arg74. c) CID of $[(\text{Ubiquitin})\cdot +10\text{H}]^{10+}$ yields loss of tyrosine side chain as most abundant fragment ion. d) Plot of side chain losses from tyrosine and arginine as a function of charge state. # neutral loss of H_2O from the molecular ion. † loss of tyrosine sidechain. Dotted arrows indicate precursor m/z.

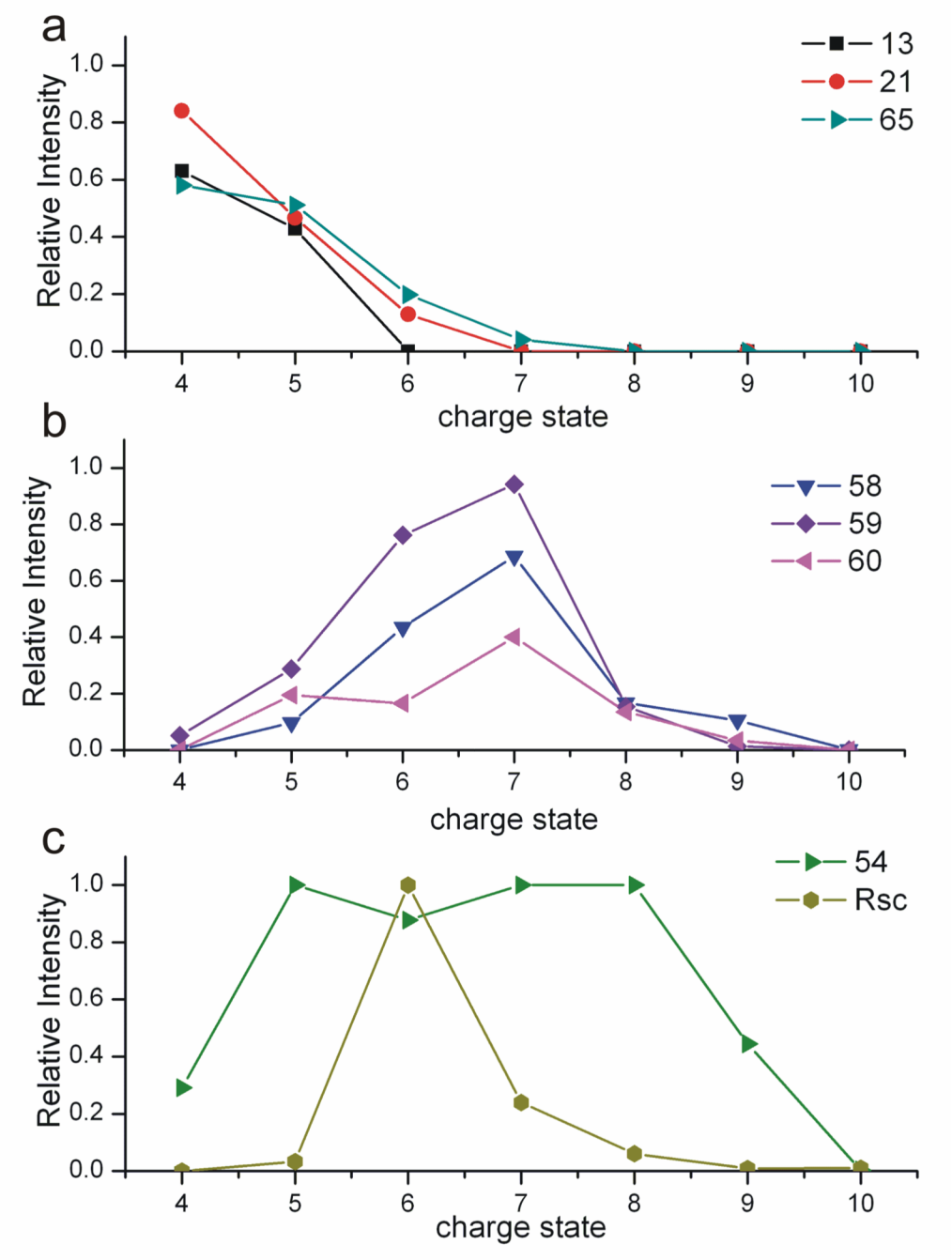

Figure 5.

Selected backbone and side chain fragmentation products as a function of charge state (a–c). Fragmentation at residues 13, 21, and 65 dominate at lower charge states (compact conformers), and disappear by the +8 charge state (a). Partially unfolded conformers are characterized by enhanced fragmentation nearby Tyr59 (b), and fragmentation at residues 54 and 72/74 (c, see text).

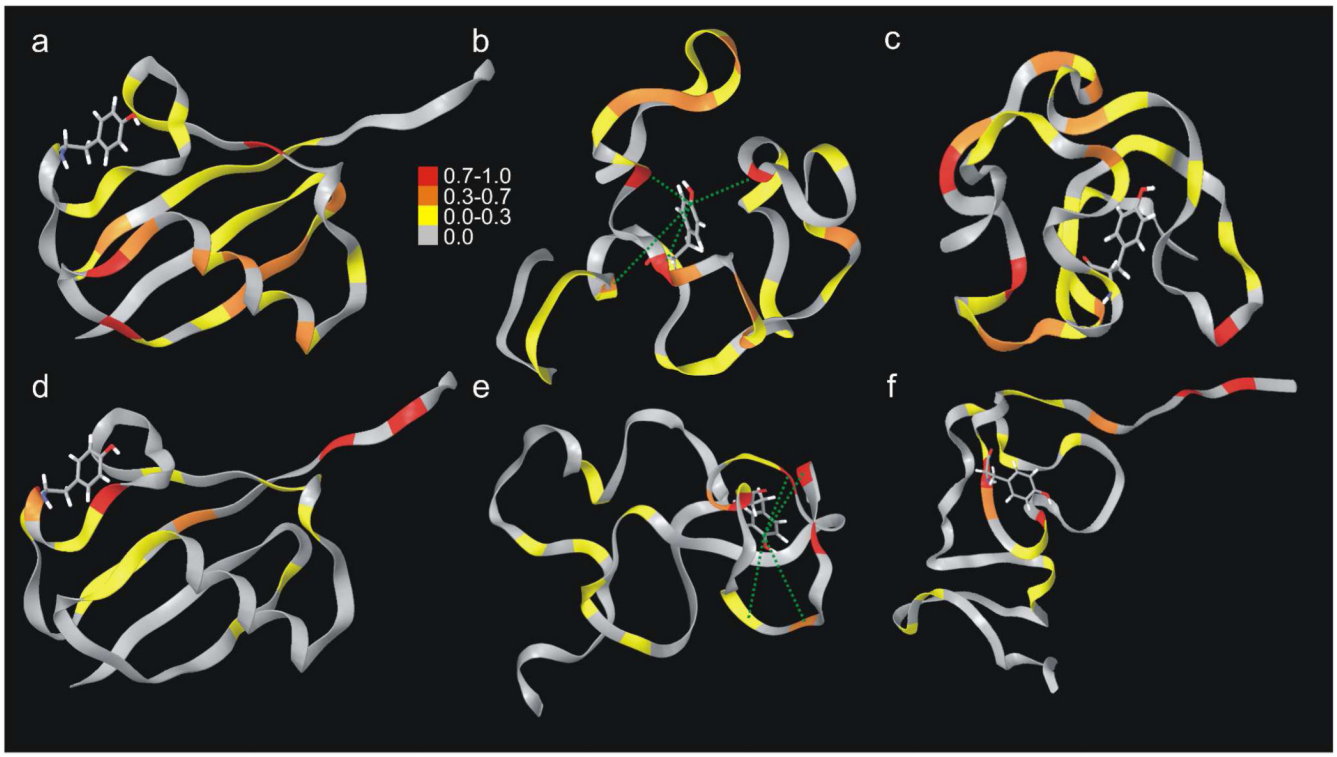

Figure 6.

a) The crystal structure of ubiquitin with color coding indicating the intensity of RDD backbone fragmentation for the +4 charge state. b) Structure of the +4 charge state of ubiquitin calculated by MDSA using distance constraints derived from experimental data, which are shown as green dotted lines. The coloring is the same as in (a). c) MDSA output without distance constraints. d) The crystal structure of ubiquitin colored by RDD fragment intensities of the +6 charge state. Arg72 and Arg74 are highlighted in red, due to the dominant arginine side chain loss observed. e, f) The output structures of a constrained and unconstrained MDSA calculation, respectively, with identical coloring as (d).

Table 1

A Comparison between the Crystal and Calculated Structures

Structure	Cross Section[a] Å²	Energy[b] kJ·mol⁻¹	Correlation with RDD[c]	Distance from Tyr59 (Å)			
				Val17	Thr22	Arg42	Thr66
+4, Crystal Structure	1059	−11165	0.30	13.1	9.3	12.5	15.1
+4, Constrained[d]	1075	−11792	0.47	7.2	6.4	6.6	7.5
+4, Unconstrained[d]	1067	−11837	0.30	10.2	19.6	14.1	18.2
				Thr55	Thr66	His68	Arg74
+6, Crystal Structure	1059	−10457	0.67	8.9	15.1	13.9	22.4
+6, Constrained[d]	1129	−11359	0.87	6.8	8.2	6.4	7.9
+6, Unconstrained[d]	1294	−11101	0.64	5.5	9.9	14.8	35.2
+6, Rearranged[e]	1053	−10982	0.78	11.7	13.7	12.5	3.8

[a] Exact hard sphere approximation

[b] Gradient-minimized MM energies calculated using the OPLS force field

[c] 1.0 indicates perfect correlation; 0.23 is score for a random structure (see text for details)

[d] MDSA

[e] MD